Origin of the c/a variation in hexagonal close-packed divalent metals

U. Häussermann[1] and S. I. Simak[2]
[1]*Department of Inorganic Chemistry, Stockholm University, S-10691 Stockholm, Sweden*
[2]*Department of Applied Physics, Chalmers University of Technology and Göteborg University, S-41296 Gothenburg, Sweden*
(Received 24 April 2001; published 10 December 2001)

The origin of the c/a variation in hcp divalent metals (Be, Mg, Zn, and Cd), which ranges from 1.568 to 1.886, has been investigated by first-principles full-potential calculations in the framework of the density functional theory. We find that the ideal hcp structure ($c/a=1.633$) is electronically unstable to c/a distortions for all elements, however the distortion driving band energy is countered by the electrostatic part of the total energy, which favors the ideal close packing. In particular, Zn and Cd with c/a ratios $>$ ideal follow the bonding principle of optimum hybridization between *s* and *p* valence bands, a situation similar to the metallic elements in the neighboring group-IIIa in the Periodic Table. For Mg the electronic instability is not effective because the electrostatic part of the total energy dominates over the band energy. However, under expansion a distortion to c/a ratios $>$ ideal occurs. Finally, Be represents a special case. Typically of second-row elements, *s* and *p* valence bands mix intimately which creates an electronic structure quite distinguished from the other divalent metals. A c/a distortion cannot improve *s*-*p* band hybridization but *p*-*p* bonding is increased for $c/a<$ ideal.

DOI: 10.1103/PhysRevB.64.245114 PACS number(s): 71.15.Nc, 71.20.Be

I. INTRODUCTION

Divalent metals with an atomic electron configuration s^2 exhibit an astonishing variety in their elemental ground state structures.[1] All prominent sphere packings typical of metal structures are present: Be, Mg, Zn, and Cd adopt the hexagonal close packed (hcp) structure, Ca and Sr the face centered cubic (fcc) packing, and Ba the body centered cubic (bcc) structure. Finally, α-Hg forms a rhombohedral structure which is related to fcc. Obviously, hybridization between the *s* valence band and conduction bands have to account for the stability of the divalent metal structures because otherwise the closed-shell s^2 configuration would result in an antibonding situation for any structural arrangement when describing bonding interactions on the level of one-electron theory.

Putting aside Hg where relativistic effects are predominant,[2] the different orbital nature of the overlapping conduction band allows for a first structural classification. For Be, Mg, Zn, and Cd *p* valence electron levels are closest to the occupied *s* levels whereas the *d* levels are energetically well separated. As a consequence, in their elemental structure *s*-*p* mixing occurs which is obviously linked to a preferred formation of the hcp structure. On the other hand, the heavier alkaline earth metals Ca, Sr, and Ba have low lying *d* levels leading to a pronounced *sp*-*d* mixing in the elemental structure. According to extensive investigations by Moriarty[3,4] the *d* band contribution stabilizes the fcc structure over the hcp structure in Ca and Sr and, moreover, its drastic increase in Ba, which approaches transition metal behavior, is leading finally to a stable bcc structure.

A closer look at the hcp metals reveals a wide range in their c/a ratio, where the lowest value of 1.568 is found for Be and the largest value of 1.886 for Cd. For Mg with a c/a ratio of 1.624 the situation corresponds virtually to the case of an ideal close packing where $c/a=\sqrt{8/3}$ (1.633). The ''structural diversity'' of those metals is also reflected in their physical properties and as examples the melting points, cohesion energies, and magnetic susceptibilities are compiled together with the corresponding c/a ratios in Table I. We may use the different (outer) core electron configurations of the atoms to organize the structures: when the atomic core consists just of *s* electrons (Be: $[s^2]s^2$) the c/a ratio is lower than 1.633, when the atomic core consists of *s* and *p* electrons (Mg: $[s^2p^6]s^2$) the c/a ratio is close to 1.633, and when the atomic core consists of *s* and *d* electrons (Zn, Cd: $[s^2d^{10}]s^2$) the c/a ratio is larger than 1.633. As a consequence it appears tempting to put down the structural differences to the different core configurations.

The number of theoretical investigations on hcp divalent metals is legion. As a selection we mention the work by Moriarty[5] who first recognized the structure dependence of the hybridization to be responsible for the large c/a ratio of Zn and Cd, the work by Singh and Papaconstantopoulos[6] on the static and electronic properties of Zn in different structural alternatives, the work by Brennan and Burdett[7] who compared the electronic structures of Ca and Zn by means of semiempirical tight-binding calculations, and the work by Novikov *et al.*[8] on the pressure dependency of the c/a ratios of Zn and Cd. Concerning structural and electronic properties of Be, e.g., Blaha and Schwarz[9] and Chou *et al.*[10] made

TABLE I. Structural and physical properties [melting point (MP), cohesion energy (E_{coh}), and molar magnetic susceptibility (χ_{mol})] of hcp divalent metals.

property	Be	Mg	Zn	Cd
c/a (Ref. 29)	1.568	1.624	1.856	1.886
MP (°C) (Ref. 26)	1290	650	421	323
E_{coh} (kJ/mol) (Ref. 26)	320	145	130	112
χ_{mol} (10^{-11} m^3/mol) (Ref. 33)	−11.5	+17.8	−11.7	−25.1
χ_{mol}-$\chi_{mol,core}$ (10^{-11} m^3/mol)	−11.0	+21.8	+1.3	+2.9

earlier contributions within the local density functional scheme. However, comparative studies of divalent metals are rare or incomplete. In the early 1970's Heine and Weaire[11] and later Hafner and Heine[12] proposed—in the context of qualitative pseudopotential theory—the distorted hcp structures in Zn and Cd being a consequence of a decreased ratio between the ionic core radius and atomic radius (R_c/R_a) compared to Mg. More recently Daniuk *et al.*[13] presented *ab initio* band structures and Fermi surfaces of Mg, Zn, and Cd, but their focus was on the comparison with other *ab initio* calculations and experiment rather than interpreting the differences in the structural properties. In the present paper we analyze in detail how hybridization of the *s* and *p* valence bands influences the c/a ratio in the hcp divalent metals and thus extend our earlier developed general bonding picture for the metallic elements of group-IIIA (Al, Ga, In, Tl).[14,15] In addition we apply the idea of expansion for establishing electronic structure relationships between isovalent metals which complements the traditional studies of structural stability as a function of compression. Our work is based on high-accuracy full-potential calculations in the framework of the density functional theory.

Computational details are given in Sec. II. Section III is devoted to the theory of band hybridization in divalent metals with hcp structure. Section IV contains the results of first-principles calculations and discussion of the structural stability of these elements. A summary and conclusions are given in Sec. V.

II. COMPUTATIONAL DETAILS

Total energy calculations for hcp Be, Mg, Zn, and Cd were performed with the full-potential linearized augmented plane wave (FLAPW) method.[28] As experimental ground state volumes V_0 we took the values reported in Ref. 29 for 298 K: V_0 (Be)$=8.110$, V_0 (Mg)$=13.418$, V_0 (Zn) $=15.214$, V_0 (Cd) $=21.599$ Å^3 per atom. The band structure of linear chains of Be, Mg, and Zn with an atomic separation of 2.255, 3.203, and 2.781 Å, respectively (average nearest neighbor distance in the respective elemental structures), were calculated by using a simple hexagonal structure where the c/a ratio has been decreased to such an extent that an array of noninteracting linear chains separated by 10 Å resulted. In full-potential techniques within density functional theory basis functions, electron densities, and potentials are calculated without any shape approximation. These methods belong to the most accurate ones to date concerning studies of structural stability. In particular we used well-converged plane wave sets with a cutoff parameter $R_{mt}K_{\max}=9.0$ for all elements. The Zn $3d$ (and Cd $4d$) states were treated as local orbitals.[30] For Be and Mg we used the local density approximation (LDA) with the exchange-correlation potential parametrization according to Perdew *et al.*[31] For Zn (and Cd), however, LDA fails to reproduce the experimental equilibrium volume and thus yields optimum c/a ratios too large in total energy vs c/a calculations at the respective experimental equilibrium volumes. It is known that the more advanced generalized gradient approximation (GGA) overcomes this problem.[8] Thus we applied the GGA according to Perdew, Burke, and Ernzerhof[32] in our calculations for Zn and Cd. The reciprocal space integrations were performed with the tetrahedron method using $972k$ points in the irreducible part of the hexagonal Brillouin zone. In order to ensure convergency several standard tests were performed, such as the effect of increasing the number of *k*-points used in the summation over the BZ, etc.

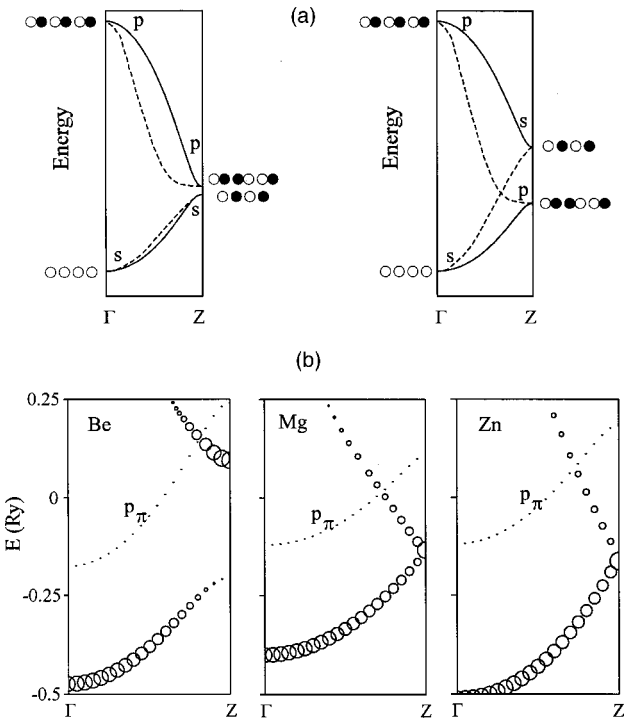

FIG. 1. (a) Schematical representation of the interaction between *s* and *p* valence bands in the band structures of main group elemental solids (based on Ref. 16). Weak interaction is shown in the left hand part, strong interaction in the right hand part. Dashed lines approximate the dispersion of the unhybridized (noninteracting) bands. The orbital combinations indicate the bonding character of the bands. (b) The band structure of linear chains of Be, Mg, and Zn atoms with atomic distances of 2.255, 3.203, and 2.781 Å, respectively. The *s* orbital character of the wave functions is proportional to the size of the circles. The unit of the energy is Ry (1 Ry ≈ 13.6 eV).

III. BAND HYBRIDIZATION

A. Model system: One-dimensional chains

The mechanism of *s*-*p* band hybridization or *s*-*p* band mixing is most easily visualized by studying a simple model system consisting of a one-dimensional chain of atoms as suggested by Burdett.[16] As schematically depicted in Fig. 1(a) the σ interacting *s* and p_z bands run oppositely along the reciprocal direction $\Gamma-Z$ and when the dispersion (band width) of the bands is large enough, their interaction leads to an opening of a hybridization gap at *Z*. Accompanied with the gap formation is a change in the bonding characteristics of the bands: the lower band becomes completely bonding whereas the upper one turns into a completely antibonding one. Thus, in the case of strong *s*-*p* mixing the

TABLE II. Energy of the atomic one-electron valence levels of the hcp divalent metals (Ref. 34).

	Be	Mg	Zn	Cd
ϵ_s (eV)	−9.32	−7.64	−9.39	−8.99
ϵ_p (eV)	−6.60	−4.93	−5.38	−5.26
$\Delta\epsilon_{sp}$ (eV)	2.72	2.71	4.01	3.73

one-dimensional chain gets maximally stabilized with an electron count corresponding to a completely filled lower band. Now we analyze the situation in chains built up by Be, Mg, or Zn atoms with atomic distances corresponding to the average nearest neighbor distance in the respective elemental structures. Figure 1(b) shows the band structures of those chains (including the degenerated band stemming form the π interacting p_x and p_y orbitals). Firstly we observe that the Be chain matches perfectly the situation of strong s-p mixing as displayed in the sketch above attaining a hybridization gap of 4 eV. In the Mg and Zn chains just weak s-p interaction takes place which is not strong enough to open a gap.

The degree of s-p mixing is dependent on the size of the energy separation between the atomic s and p levels ($\Delta\epsilon_{sp}$) and on the size of the dispersion of the s and p bands. The dispersion of the bands is firstly determined by the size of the overlap between the atomic orbitals and secondly by how strongly the valence electrons are bonded to the core of the free atom (which is reflected by the energies of the atomic levels ϵ_s and ϵ_p). Comparing bands resulting from the same valence state of different elements (e.g., Be $2s$ and Mg $3s$) the state lower in energy will produce the more dispersed band, provided that the amount of nearest neighbor overlap between the corresponding orbitals [e.g., Be ($2s$-$2s$) and Mg ($3s$-$3s$)] is not too different. Thus, if only referring to the trend in the atomic energies of the s and p levels and their separation (summarized in Table II) the electronic structure of the chains can be established qualitatively. Be has low lying s and p orbital energies giving rise to a large dispersion of the corresponding s and p bands (this is also recognized in the p-π bands). Additionally $\Delta\epsilon_{sp}$ is small. As a consequence strong s-p mixing occurs which is accompanied with the formation of a large hybridization gap separating the completely bonding lower σ band from the antibonding upper one. The s and p bands of Mg have a low dispersion (higher s and p orbital energies compared to Be) but the quite small $\Delta\epsilon_{sp}$ still ensures a moderate s-p mixing which, however, is too weak for producing a hybridization gap. Finally, in Zn the s and p bands have a large dispersion but the also large $\Delta\epsilon_{sp}$ prevents substantial s-p mixing and thus Zn attains a similar state of hybridization as Mg. For the latter metals the σ bands are grown together and s-s antibonding and p-p bonding states mix around the edge Z of the BZ. The simple one-dimensional chain model structure already provides essential information on the dispersion of the valence bands and the amount of s-p hybridization for the elements considered, which—as we will see—also holds for the hcp structure.

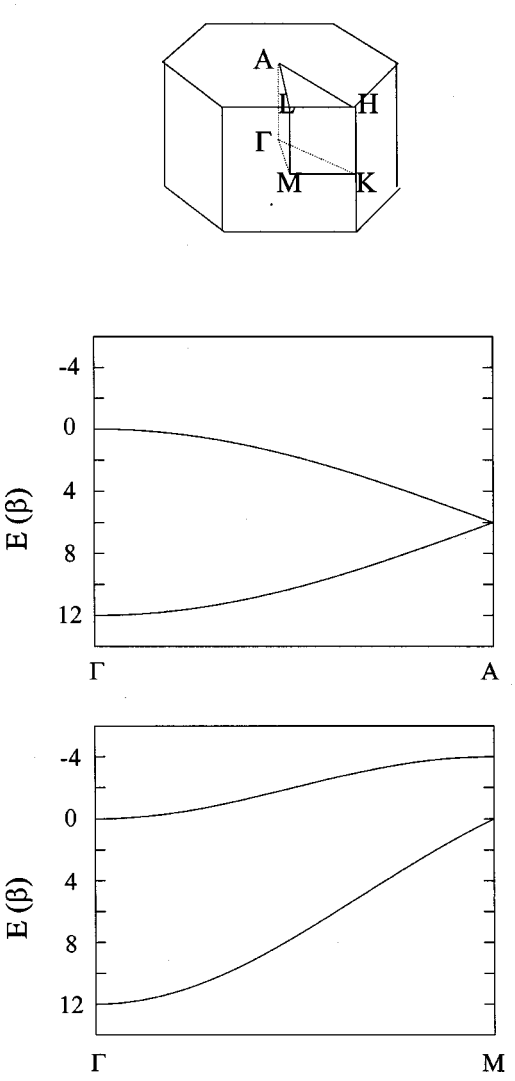

FIG. 2. The upper part shows the Brillouin zone of the hcp structure with symmetry points specified. In the lower part the s band topologies along Γ-A and Γ-M as obtained from the analytical expression within tight-binding (Hückel) theory (Ref. 17). The unit of the energy is the Hückel interaction integral β (<0).

B. The (ideal) hcp structure

We first have a look at the s-s interactions in the hcp structure. The two atoms in the unit cell of hcp will produce two s bands. It is easy to study the topology of these bands by using simple tight-binding (TB) Hückel theory where it is possible to obtain an analytic expression of the s band dispersion $\epsilon_s(k)$.[17] In Fig. 2 the directions Γ-M and Γ-A are displayed together with the Brillouin zone (BZ). These directions give an impression (but not a complete picture) of interlayer and intralayer bonding, respectively. In Fig. 3 the s orbital combinations at the symmetry points Γ, A, and M are shown. Following the lower band from Γ to A it turns from being both, completely intralayer and interlayer bonding at Γ (wave function Γ_{s1}, 12 bonding nearest neighbor contacts result in a Hückel energy $\epsilon=12\beta$) to being intralayer bonding and nonbonding between the layers at A (wave function $A_s, \epsilon=6\beta$). At A the upper and lower s band are degenerate.

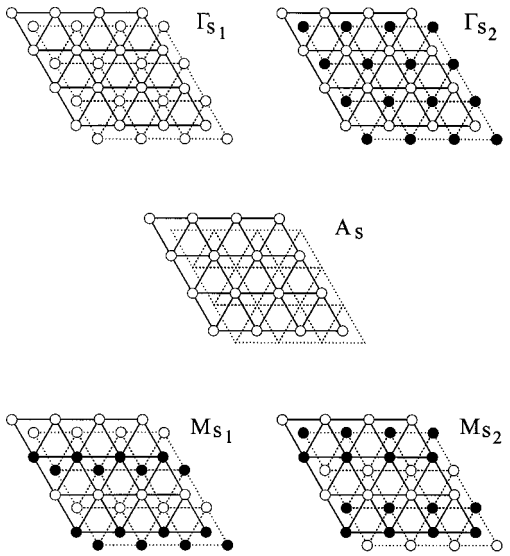

FIG. 3. *s* orbital combinations at the symmetry points Γ, *A*, and *M*.

Departing from *A* the upper band evolves more and more interlayer antibonding and at Γ the wave function becomes competely antibonding between the layers [wave function Γ_{s2}, $\epsilon=0$ (6 bonding and 6 antibonding nearest neighbor contacts)]. Along the direction Γ-*M* the lower band develops from being completely bonding (Γ_{s1}) into a situation with two bonding and four antibonding contacts within the layers and 4 bonding and two antibonding interactions between the layers [wave function M_{s1}, $\epsilon=0$ (nett nonbonding)]. The upper band starts off the interlayer bonding and intralayer antibonding combination at Γ (Γ_{s2}) and ends at *M* with two bonding and 4 antibonding contacts both within and between the layers [wave function M_{s2}, $\epsilon=-4\beta$ (nett antibonding)].

Clearly, when just considering *s*-*s* interactions the hcp structure does not provide a stable arrangement for the electron count of divalent metals and thus the mechanism of *s*-*p* band mixing has to release unfavorable *s*-*s* antibonding states above the Fermi level. In this respect the direction Γ-*A* is especially instructive because it resembles the situation of the σ interacting *s* and p_z band in a linear chain. Along Γ-*A* the p_z bands in hcp have the same topology as the *s* bands: Both types of bands are completely intralayer bonding (the interaction of the *s* bands is of σ type and that of the p_z bands of π type) and changes the interlayer bonding characteristics from completely bonding in the lower band at Γ [wave functions Γ_{s1} (Fig. 3) and Γ_{p_z1} (Fig. 4)] to nonbonding at *A*, and form nonbonding at *A* in the upper band to antibonding at Γ [wave functions Γ_{s2} (Fig. 3) and Γ_{p_z2} (Fig. 4)]. Thus, the two *s* and two p_z bands in the section Γ-*A* of hcp mirror the *s* and p_z band topology in the one-dimensional chain after having folded the bands [doubling of the chain unit cell, see Fig. 1(a)]. As for the linear chain *s*-*p* band mixing along Γ-*A* in hcp can occur when the widths of the bands are large enough. Then their interaction leads to the opening of a hybridization gap at Γ where the top of the upper band changes its bonding characteristics from interlayer *s*-*s* antibonding (Γ_{s2}) into interlayer *p*-*p* bonding (Γ_{p_z1}). In the next step we analyze the accurate and extended *ab initio* band structures for Be, Mg, and Zn in the ideal hcp structure at their respective experimental ground state volumes V_0. They are shown, together with the *s*, p_z, and $p_x(p_y)$ orbital character of the bands and the corresponding density of states (DOS) curves in Figs. 5–7. We do not present results for Cd because the band structure of this element is very similar to that of Zn.

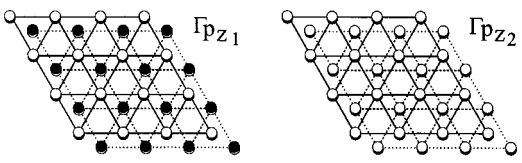

FIG. 4. p_z orbital combinations at the symmetry point Γ.

For beryllium [Fig. 5(a)] we notice large *s*-*p* hybridization (as expected from the linear chain results) which effectively raises all the *s*-*s* antibonding parts of the bands above the Fermi level. This is distinctively seen along the line Γ-*A* (s-p_z hybridization) and in the plane *A*-*H*-*L* [s-$p_x(p_y)$ hybridization]. Because the resulting hybridization gaps—with sizes up to several eV—coincide with the Fermi level they sum up to a pronounced pseudogap (almost a real band gap) at the Fermi level in the DOS [Fig. 5(b)]. Note, that hybridization gaps in three-dimensional structures are usually local band gaps (i.e., they occur for a particular direction or plane in the BZ). In Fig. 5(b) it is clearly seen that the *s* state contribution to the DOS at the Fermi level is virtually zero and that the (few) bands crossing the Fermi level have almost exclusively *p* character.

For magnesium [Fig. 6(a)] *s*-*p* mixing is considerably weaker than for Be. The small hybridization gaps (with sizes of some tenths of an eV) either are located above or below the Fermi level (at Γ, *L*, *H*, and about halfway between Γ and *M*). It is remarkable how well the topology of the *s* bands along Γ-*A* and Γ-*M* resemble those of the simple TB bands (see Fig. 2). This is the case even for the high lying upper *s* band along Γ-*M* (Γ_{s2}-M_{s2}). At Γ the bottom of this band (which is intralayer bonding and interlayer antibonding) is situated below the Fermi level (for Be it is raised above E_F). Towards *M* with increasing energy it turns more and more antibonding. About halfway along Γ-*M* interaction with the downward running $p_x(p_y)$ band takes place which opens a gap above the Fermi level and disrupts the *s* band topology. The DOS of Mg [Fig. 6(b)] exhibits parabolic behavior until -1.5 eV below the Fermi level where structuring due to *s*-*p* hybridization takes place. The location of the hybridization gaps below and above the Fermi level coincide with the dips in the DOS around the Fermi level.

The band structure of zinc [Fig. 7(a)] resembles that of Mg, especially around the Fermi level—however, the sizes of the hybridization gaps are larger (in the range of 1 eV). This gives rise to a pronounced well in the DOS slightly below the Fermi level [Fig. 7(b)]. Most conspicuous is the occurrence of the $3d$ bands at an energy of -8 eV below

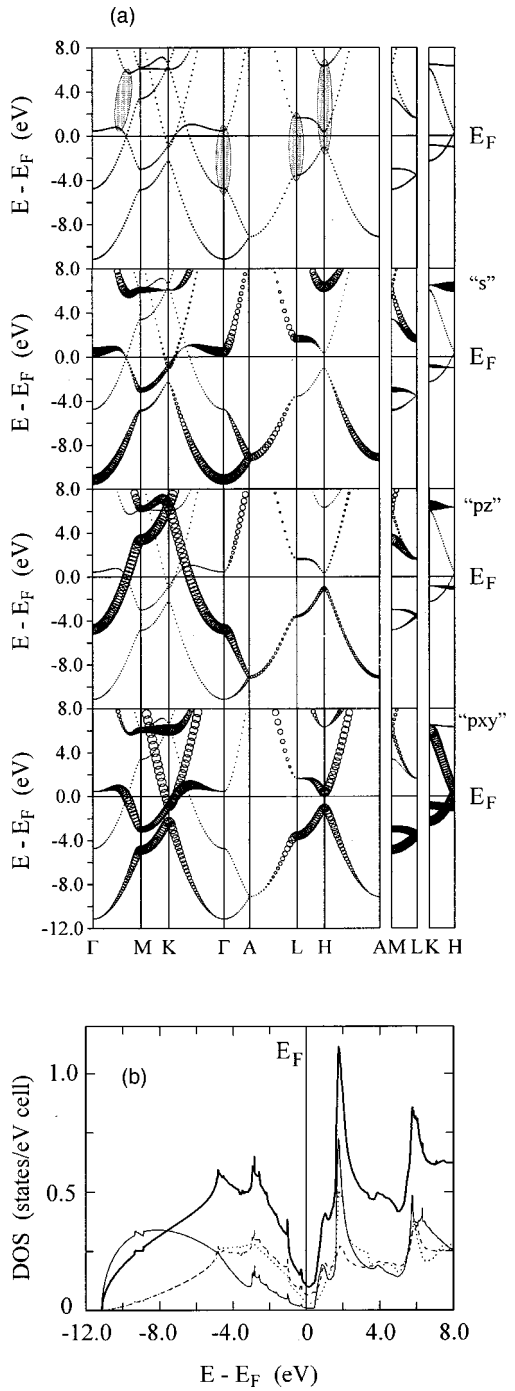

FIG. 5. (a) The top panel depicts the band structure of Be in the ideal hcp structure at the experimental ground state volume. Additionally, important s-p hybridization gaps are indicated by grey areas. In the following panels the s, p_z, and $p_x(p_y)$ character of the wave function, which is proportional to the size of the circles, is shown. (b) The total density of states (bold line) together with the s (continuous line), p_z (dotted line), and $p_x(p_y)$ orbital (dashed lines) contributions of hcp Be. For clarity, the orbital contributions to the DOS have been multiplied by a factor 3 with respect to the total DOS.

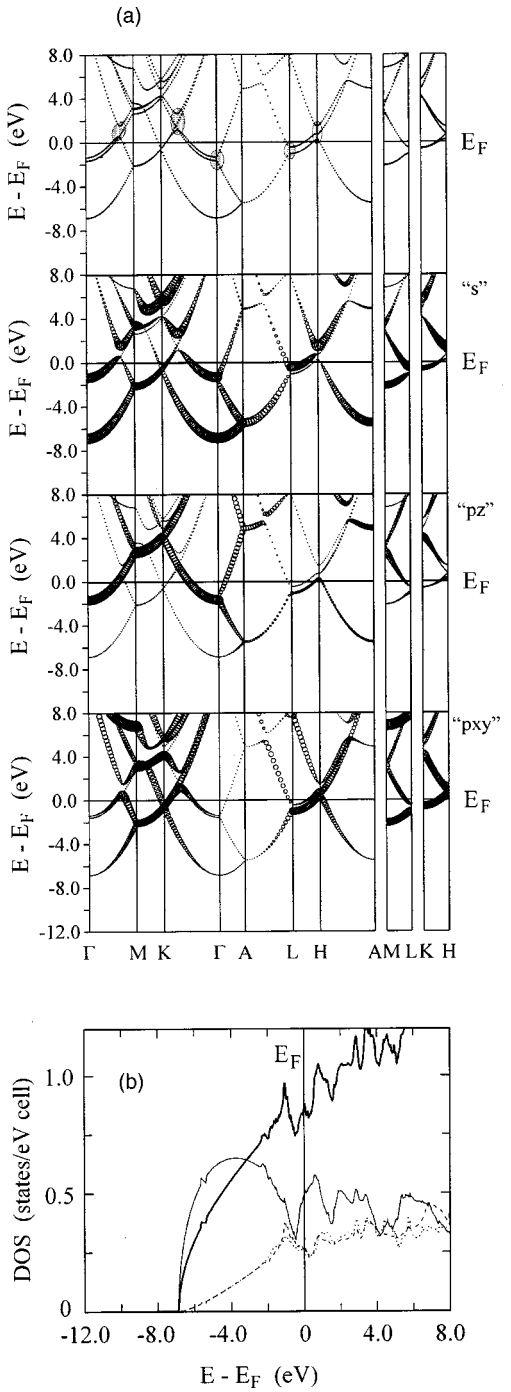

FIG. 6. The energy band structure (a) and density of states (b) of Mg in the ideal hcp structure at the experimental ground state volume. See caption of Fig. 5 for detailed explanation.

the Fermi level which are confined to a narrow range of about 1.8 eV. (For Cd the $4d$ states are just touching the bottom of the $5s$ valence band.[13]) Recently, it has been argued that the Zn $3d$ states play an important role in stabilizing the distorted hcp structure.[6] However, those states do not influence the band structure around the Fermi level which especially is the case for even more hcp distorted Cd with well localized $4d$ (pseudocore) states. We want to show that the occupied d states indirectly influence the stability of hcp Zn and hcp Cd by affecting the energy of the atomic valence levels ϵ_s and ϵ_p. And those energies predominantly determine the amount of s-p mixing which, as we will see later

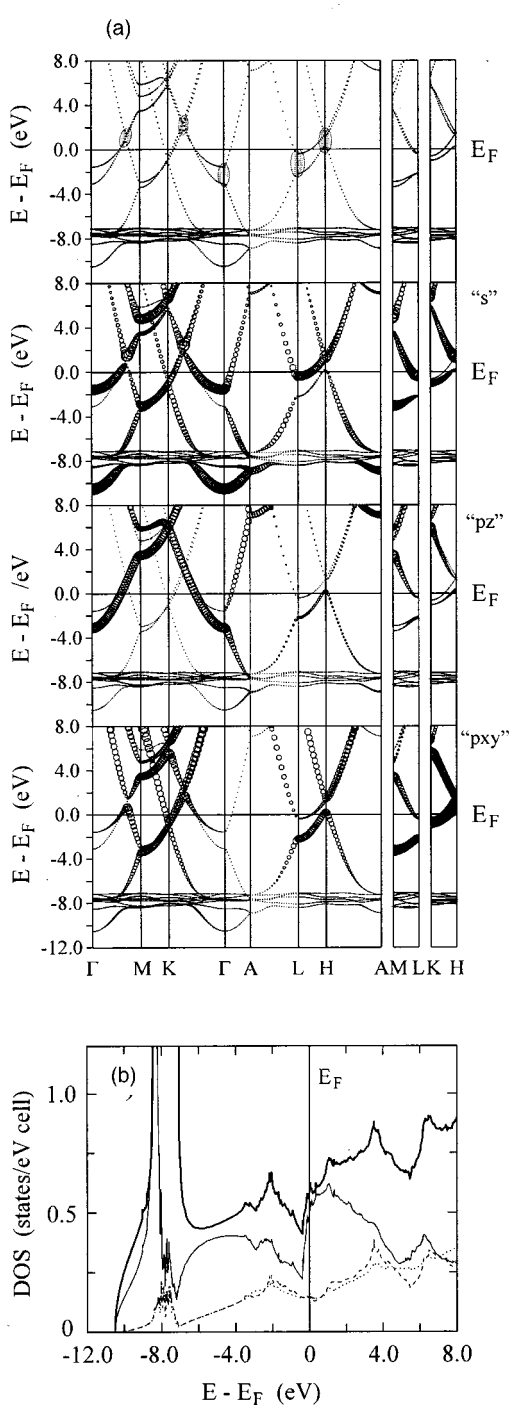

FIG. 7. The energy band structure (a) and density of states (b) of Zn in the ideal hcp structure at the experimental ground state volume. See caption of Fig. 5 for detailed explanation.

on, is the direct origin of the hcp distorted structures of Zn and Cd.

In conclusion, the hcp divalent metals realize astonishingly different electronic structures for the same arrangement of atoms and the same number of valence electrons. This can simply be attributed to the different degree of *s*-*p* band mixing expressed by those elements. In the final step we analyze if and how the different c/a ratios of the hcp divalent metals are connected with *s*-*p* hybridization.

IV. STRUCTURAL STABILITY

A. The ground state volume

The problem of structural stability of elemental solids is preferably tackled by dividing the total energy into the band energy E^{band}, which represents the sum over the occupied one-electron states, and a part containing the remaining contributions, of which the electrostatic (Madelung) energy is the most significant. The band energy can to a good approximation be reduced to the contribution of the valence electrons $E^{\text{band}}=\int_{\epsilon_b}^{\epsilon_F}\epsilon\,\text{DOS}(\epsilon)d\epsilon$, where ϵ_b denotes the bottom of the valence band, ϵ_F is the Fermi level, and DOS (ϵ) the density of states of the valence electrons. E^{band} favors the formation of open packed structures in which the atoms are closer to each other and thus covalent bonding can be realized. The electrostatic contributions (summarized as E^{Mad}) display an antagonistic behavior with the tendency to stabilize high-symmetry close-packed structures. For most of the main group elements from groups IVa to VIIa E^{band} is determining the elemental structures which is manifested in the validity of valence rules which link electron counts to particular geometrical arrangements of atoms. The decrease of the number of valence electrons to three in group-IIIa terminates the clear link between electron count and geometrical structure in elemental solids leading to a delicate interplay of E^{band} and E^{Mad} which is responsible for the occurrence of the open packed metallic structures of Ga and In.[14,18,19] For the divalent metals with an electron count of two E^{Mad} could be expected to dominate over E^{band}. However, the large range in the c/a ratios of the hcp divalent metals indicates that E^{band} still influences structural stability.

Figure 8 shows the total energy and the band energy of Be, Mg, and Zn as a function of c/a at the respective experimental ground state volumes V_0 of the elements. Two important results emerge: first full-potential calculations quite accurately reproduce the experimental c/a ratios of those elements, i.e., the experimental values are obtained for Be and Mg (see Table I) and a value just slightly higher for Zn (1.878 compared to 1.856). Secondly, for divalent metals the ideal hcp structure appears unstable against c/a distortions for electronic reasons because for all three elements the band energy does not attain a minimum at $c/a=1.633$. A closer look at the changes of the electronic structures under distortion reveals the reason behind this electronic instability. Figure 9 displays the band structures of Be, Mg, and Zn at one selected $c/a<$ ideal and $c/a>$ ideal each (see Figs. 5–7 where the corresponding band structures at ideal c/a are shown). In Fig. 10 the DOS at different c/a ratios are collected and compared with the DOS at ideal c/a.

For beryllium the *s*-*p* hybridization gaps are already located at the Fermi level for the ideal hcp structure. This corresponds to a situation of optimum *s*-*p* hybridization where *s*-*s* antibonding states have been exchanged for *p*-*p* bonding ones for the largest possible part of the BZ. A distortion in any of the two directions $c/a<$ ideal and $c/a>$ ideal worsens the stabilizing effect of *s*-*p* mixing. This is especially seen for a distortion to larger c/a which eventually lowers the bottom of the third valence band at Γ (Γ_{s2}),

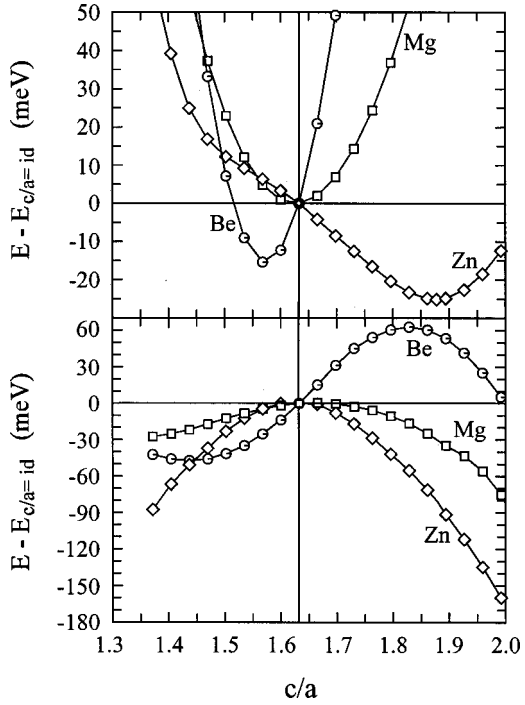

FIG. 8. The upper panel shows the total energy as a function of c/a for Be (circles), Mg (squares), and Zn (diamonds) (at the respective experimental ground state volumes) with respect to the ideal hcp structure. The lower panel shows the corresponding variation of the valence electron parts of the band energy. For Zn the values have been divided by a factor 10 in order to fit the energy range of the graph. The c/a ratio for ideal hcp is marked.

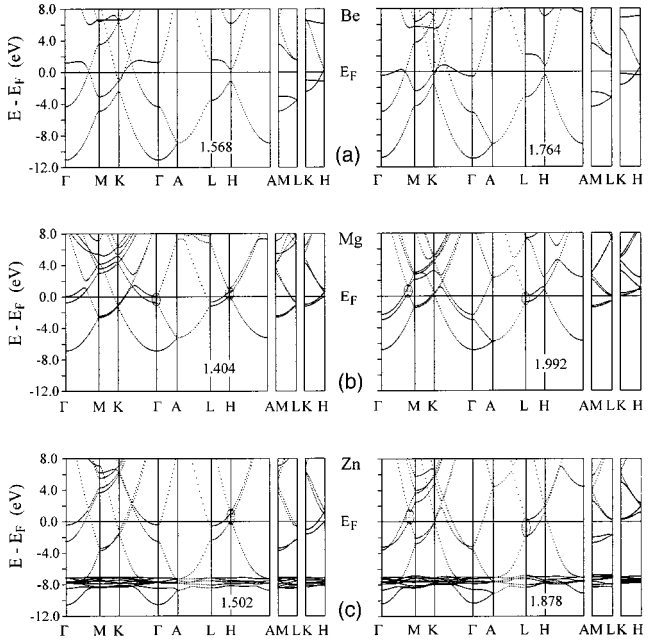

FIG. 9. (a) The band structure of hcp Be for $c/a=1.568$ (left) and $c/a=1.764$ (right) at the experimental ground state volume V_0. (b) The band structure of hcp Mg for $c/a=1.404$ (left) and $c/a=1.992$ (right) at V_0. (c) The band structure of hcp Zn for $c/a=1.502$ (left) and $c/a=1.878$ (right) at V_0. In (b) and (c) s-p hybridization gaps at the Fermi level are marked by grey areas.

which is interlayer antibonding along Γ-A due to s-p hybridization, below the Fermi level. Thus, the driving force behind the distortion of hcp Be is not directly connected to s-p hybridization. We attribute it to the occurrence of very flat bands with basically $p_x(p_y)$ character slightly below the Fermi level. They can be recognized as spiky singularities in the DOS [Fig. 10(a)] and one of these bands is clearly seen in the direction K-H of the presented band structures [Figs. 5(a), 9(a)]. The change of the position of a flat band has a large effect to E^{band}. For Be a decrease of the c/a ratio below the ideal value [see Figs. 9(a) and 10(a)] lowers the energy of the flat bands and thus E^{band}. However, deviations from ideal c/a cannot become too large because of the countering electrostatic contributions to the total energy which increase rapidly with increasing distortion. The occurrence of flat bands is actually an indirect consequence of strong s-p mixing. Considering again the flat band along K-H we observe that its weak dispersion arises from the large hybridization gap at H produced along the direction A-H. When comparing with the corresponding band in the band structures of Mg and Zn which exhibit a ''normal'' dispersion behavior (i.e., bottom at K and top at H) it is seen that for Be the energy at H is lowered to such an extent that it becomes almost the same as at K.

For magnesium the maximum of E^{band} is obtained at the ideal c/a ratio and thus distortion in any direction is lowering E^{band}. In contrast to Be, here distortion is accompanied by an increase of the amount of s-p mixing and as a consequence s-p hybridization gaps are put at the Fermi level. When decreasing c/a the s-p_z hybridization gap produced along A-Γ and the s-$p_x(p_y)$ gap produced along A-H, which are situated below and above the Fermi level at ideal c/a respectively, move oppositely and at $c/a=1.4$ they coincide with the Fermi level. For the other distortion direction the hybridization gap located between Γ and M (above the Fermi level at ideal c/a) and that at L (below the Fermi level at ideal c/a) are moved simultaneously to the Fermi level which they enter for a c/a around 2. In the DOS [Fig. 10(b)] we can recognize the two favorable situations at $c/a=1.4$ and $c/a=2$ as a splitting of states around the Fermi level which thus becomes located in dips where the density of states is considerably reduced compared to the case of ideal c/a. However, for Mg the increase of s-p hybridization and thus the lowering of E^{band} is not structure determining and the ideal hcp structure is obtained for electrostatic reasons.

Finally, for zinc (and Cd) the influence of c/a variations on the band structure is similar as for Mg: in both distortion directions E^{band} is decreased and the rate of s-p mixing increased. As for Mg a decrease of the c/a ratio especially affects the hybridization gaps at Γ and H. However, for Zn the movement of those gaps is not exactly synchronized and the hybridization gap at H enters the Fermi level before the one at Γ. On the other hand, for distortions to higher c/a there is a concerted movement of the hybridization gap located between Γ and M (above the Fermi level at ideal c/a) and that at L (below the Fermi level at ideal c/a) which enter the Fermi level at the same time at a ratio $c/a=1.878$. This

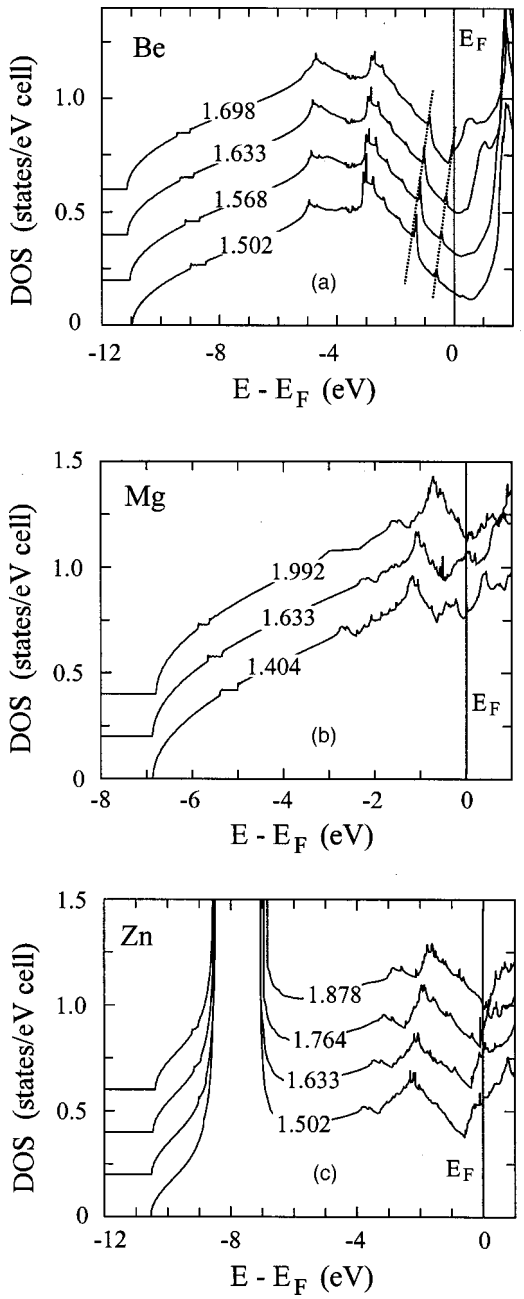

FIG. 10. (a) The total density of states (DOS) of Be at the experimental ground state volume V_0 for the c/a ratios 1.502, 1.568, 1.633, and 1.698. Note the energy changes of the spikes below the Fermi level corresponding to flat bands (marked by broken lines). (b) DOS for Mg at V_0 for the c/a ratios 1.404, 1.633, and 1.992. (c) DOS for Zn at V_0 for the c/a ratios 1.502, 1.633, 1.764, and 1.878.

ratio corresponds to the calculated optimum c/a ratio where the total energy is lowest. In the DOS [Fig. 10(c)] we observe that the distortion to higher c/a puts the Fermi level into the pronounced well produced by the hybridization gaps (this well is below the Fermi level for ideal c/a). The other distortion direction does not yield a dip at the Fermi level in the DOS as obtained for Mg, because the gaps at Γ and H do not become coinciding with the Fermi level simultaneously.

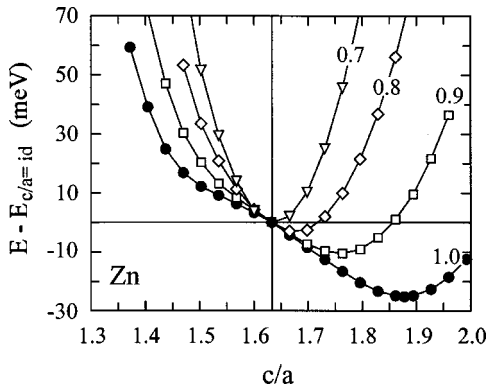

FIG. 11. Total energy as a function of c/a and volume ($V/V_0 = 0.7, 0.8, 0.9, 1.0$) for Zn with respect to the ideal hcp structure (the ground state volume curve is highlighted by filled circles).

According to the theory of electronic topological transitions (ETT) such a stabilizing dip at the Fermi level—and thus a possible electronically driven structural transition—can only occur when at least two hybridization gaps enter the Fermi level *simultaneously and from opposite directions* by a structural change.[20]

In conclusion we observe that for Zn (and Cd) the distorted hcp structure appears as a consequence of the optimization of s-p mixing of the valence bands which exchanges s-s antibonding states below the Fermi level for p-p bonding ones and thus lowers E^{band}. For Mg this optimization of s-p mixing is not structure determining because the electrostatic part of the total energy dominates over E^{band}. Be already attains in the ideal hcp structure a situation of optimum s-p hybridization which creates as a by-product flat bands with $p_x(p_y)$ character below the Fermi level. The lowering of those flat bands drives the distortion to $c/a <$ ideal for hcp Be.

B. The effect of volume variations

The two total energy contributions E^{band} and E^{Mad} behave differently when the volume V/V_0 is varied. Due to its largely Coulombic nature E^{Mad} varies approximately as $[1/(V/V_0)]^{1/3}$ whereas E^{band} alters in a more complicated way, dependent on how the bandwidths of the different valence bands change with volume. For many elements E^{Mad} increases relative to E^{band} under compression and close packed structures are obtained as high pressure modifications. However, there are examples [e.g., the heavier alkali metals or Ca (Ref. 21)] where actually transitions to more open packed structures are found at elevated pressures. In such cases the valence state of the elements changes under compression (for the above mentioned examples a s-d transition occurs) which makes E^{band} to alter discontinuously. For Zn the occupied $3d$ states prevent the $4d$ states of becoming valence states and it is known that the distorted hcp structure transforms to an ideal close packing under compression. Indeed, as it is shown in Fig. 11, the optimum c/a ratio of Zn decreases under pressure and at $V/V_0 \approx 0.7$ attains a value close to ideal hcp after which it stays roughly constant. This is close to the experimental result where the ideal

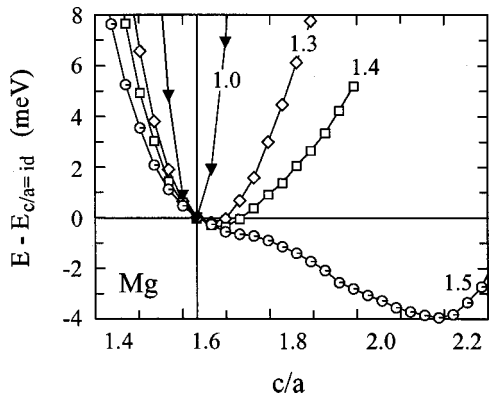

FIG. 12. Total energy as a function of c/a and volume ($V/V_0 = 1.0,1.3,1.4,1.5$) for Mg with respect to the ideal hcp structure (the ground state volume curve is highlighted by filled triangles).

c/a ratio is approached at volumes slightly below $V/V_0 = 0.8$ (Ref. 22) (corresponding to an external pressure of about 250 kbar) and has already been the subject of theoretical investigations.[23,8]

For Mg at its ground state volume E^{Mad} dominates over E^{band} which corresponds to the situation of Zn under high pressure (reduced volume). If E^{Mad} decreases faster as E^{band} with increasing volume one could speculate that Mg might transform to a distorted hcp structure under *expansion*, i.e., at a volume where the distortion driving electronic part of the total energy overcomes the electrostatic part. From a theoretical point of view there is no conceptual difficulty with a state of expansion, it is simply the negative direction on the pressure axis. Moreover, this idea offers a beautiful complement to the traditional studies of structural stability as a function of compression because it enlarges the possibility of detecting electronic structure relationships.[24] In Fig. 12 we present the result of the c/a variation of Mg under expansion. Until volumes $V/V_0 < 1.3$ the ideal c/a ratio is maintained, between $V/V_0 = 1.3$ and 1.4 a distortion towards a higher c/a value becomes apparent which develops gradually into a total energy vs c/a curve mirroring that of Zn at its ground state volume (see Fig. 11). Thus, Mg and Zn behave in an opposite way when varying volume: under compression Zn transforms to an ideal hcp structure which Mg adopts at ambient conditions and Mg under expansion transforms to a distorted hcp structure which Zn adopts at ambient conditions.

V. CONCLUSIONS

The divalent metals Be, Mg, Zn, and Cd with the hcp structure are rather heterogeneous concerning their c/a ratios ranging from 1.568 (Be) to 1.886 (Cd) and their physical properties (Table I). We analyzed in detail the origin of this c/a variation and found that it is closely connected to firstly the different extent of s-p mixing which can be expressed by those elements and secondly a delicate interplay between the total energy contributions band energy E^{band} and electrostatic (Madelung) energy E^{Mad}, which is typical for elements at the borderline between metals and nonmetals. With the exception of Be the divalent metals behave as the metallic elements of group-IIIa (Refs. 14,15,18,19) adopting a ground state structure in which s-p mixing of the valence bands (and thus E^{band}) is optimized with respect to the electrostatic contributions to the total energy.

In particular, we find for magnesium that E^{Mad} overrides the distortion driving band energy and the ideal hcp structure is obtained for electrostatic reasons. However, under expansion the relative significance of E^{band} and E^{Mad} to structural stability changes and a distortion to c/a ratios $>$ ideal appears above a volume $V/V_0 = 1.4$.

For the more electronegative metals zinc and Cd this distortion already occurs at ambient conditions. The stronger influence of E^{band} on structural stability in those metals is a consequence of the lower lying valence levels ϵ_s and ϵ_p compared to Mg. The filled d shell in the core increases the effective nuclear charge (especially in the case of the first d-shell $3d$) primarily for s valence electrons and partly for p valence electrons.[25] Characteristic for the electronic structures of hcp distorted Zn and Cd is a well in the DOS at the Fermi level produced by several hybridization gaps coinciding at this energy. Mg, Zn, and Cd are Pauli paramagnets (the latter after correcting for the Landau and Larmor diamagnetic susceptibility contributions of the cores). However, whereas the Pauli paramagnetism of Mg is quite pronounced the one of Zn and Cd is very weak. Since the Pauli paramagnetic susceptibilities mirror the value of the valence DOS at the Fermi level[26] we readily understand the poor Pauli paramagnetism of Zn and Cd compared to Mg.

Beryllium is distinguished from the other divalent metals. The core configuration $[1s^2]$ provides low lying s and p valence states with a small energetic separation. The latter fact is due to the absence of core p electrons and their corresponding repulsive influence on the valence $2p$ states.[27] Thus, in hcp Be s and p valence bands mix intimately and as a consequence of the effective s-p hybridization a pronounced pseudogap at the Fermi level is created which is responsible for the astonishing high diamagnetism. (Note, that in the neighboring element boron a real band gap at the Fermi level is realized in semiconducting α-B.) Additionally, for Be all possible s-s antibonding states are replaced for p-p bonding ones below the Fermi level leading to a situation with basically just bonding occupied states. Thus, compared to the other divalent metals Be has an exceptional high melting point and energy of cohesion. Finally, the decrease of E^{band} by a distortion $c/a <$ ideal does not parallel an increase of s-p mixing, but rather increases p-p bonding by a lowering of flat bands with $p_x(p_y)$ character.

ACKNOWLEDGMENTS

This work was supported by the Swedish National Science Research Council (NFR), Materials Consortium "ATOMICS" and the Göran Gustafsson Foundation. We thank I. A. Abrikosov, Uppsala University, for valuable discussions.

[1] J. Donohue, *The Structure of the Elements* (Wiley, New York, 1974).
[2] P.P. Singh, Phys. Rev. B **49**, 4954 (1994); see also Phys. Lett. A **131**, 41 (1988), for the discussion of Hg at high pressure.
[3] J.A. Moriarty, Phys. Rev. B **8**, 1338 (1973).
[4] J.A. Moriarty, Phys. Rev. B **34**, 6738 (1986).
[5] J.A. Moriarty, Phys. Rev. B **26**, 1754 (1982); J. Quantum Chem. **17**, 541 (1983).
[6] D. Singh and D.A. Papaconstantopoulos, Phys. Rev. B **42**, 8885 (1990).
[7] T.D. Brennan and J.K. Burdett, Inorg. Chem. **32**, 746 (1993).
[8] D.L. Novikov, A.J. Freeman, N.E. Christensen, A. Svane, and C.O. Rodriguez, Phys. Rev. B **56**, 7206 (1997).
[9] P. Blaha and K. Schwarz, J. Phys. F: Met. Phys. **17**, 899 (1987).
[10] M.Y. Chou, P.K. Lam, and M.L. Cohen, Phys. Rev. B **28**, 4179 (1983).
[11] V. Heine and D. Weaire, Solid State Phys. **24**, 249 (1970).
[12] J. Hafner and V. Heine, J. Phys. F: Met. Phys. **13**, 2479 (1983).
[13] S. Daniuk, T. Jarlborg, G. Kontrym-Sznajd, J. Majsnerowski, and H. Stachowiak, J. Phys.: Condens. Matter **1**, 8397 (1989).
[14] U. Häussermann, S.I. Simak, R. Ahuja, and B. Johansson, Angew. Chem. **112**, 1301 (2000); Angew. Chem. Int. Ed. Engl. **39**, 1246 (2000).
[15] S.I. Simak, U. Häussermann, R. Ahuja, S. Lidin, and B. Johansson, Phys. Rev. Lett. **85**, 142 (2000).
[16] J. K. Burdett, *Chemical Bonding in Solids* (Oxford University Press, Oxford, 1995).
[17] J.R. Reitz, Solid State Phys. **1**, 2 (1955).
[18] U. Häussermann, S.I. Simak, I.A. Abrikosov, and S. Lidin, Chem. Eur. J. **3**, 904 (1997).
[19] U. Häussermann, S.I. Simak, R. Ahuja, B. Johansson, and S. Lidin, Angew. Chem. **111**, 2155 (1999); Angew. Chem. Int. Ed. Engl. **38**, 2017 (1999).
[20] M.I. Katsnelson, I.I. Naumov, and A.V. Trefilov, Phase Transitions **49**, 143 (1994).
[21] U. Schwarz, K. Takemura, M. Hanfland, and K. Syassen, Phys. Rev. Lett. **81**, 2711 (1998); U. Schwarz, A. Grzechnik, K. Syassen, I. Loa, and M. Hanfland, *ibid.* **83**, 4085 (1999); H. Olijnyk and W.B. Holzapfel, Phys. Lett. **100A**, 191 (1984); R. Ahuja, O. Eriksson, J.M. Wills, and B. Johansson, Phys. Rev. Lett. **75**, 3473 (1995).
[22] O. Schulte and W.B. Holzapfel, Phys. Rev. B **53**, 569 (1996).
[23] L. Fast, R. Ahuja, L. Nordström, J.M. Wills, B. Johansson, and O. Eriksson, Phys. Rev. Lett. **79**, 2301 (1997).
[24] P. Söderlind, O. Eriksson, B. Johansson, J.M. Wills, and A.M. Boring, Nature (London) **374**, 524 (1995).
[25] J. E. Huheey, E. A. Keiter, and R. L. Keiter, *Inorganic Chemistry: Principles of Structure and Reactivity* (Harper Collins College Publishers, New York, 1993).
[26] C. Kittel, *Introduction to Solid State Chemistry* (Wiley, New York, 1996).
[27] D. G. Pettifor, *Bonding and Structure of Molecules and Solids* (Clarendon Press, Oxford, 1995).
[28] P. Blaha, K. Schwarz, and J. Luitz, Program WIEN97: A Full Potential Linearized Augmented Plane Wave Package for Calculating Crystal Properties (K. Schwarz, Techn. Universität Wien, Austria, 1999).
[29] *Crystal Structures and Lattice Parameters of the Metallic Elements: Binary Alloy Phase Diagrams*, 2nd ed. (ASM International, Materials Park, OH, 1996).
[30] In order to improve the linearization (i.e,. to increase the flexibility of the basis, which is recommended for the *d* states of late transition metals) and to make possible a consistent treatment of semicore and valence states in one energy window additional basis function can be added. They are called ''local orbitals'' [D. Singh, Phys. Rev. B **43**, 6388 (1991)] and consist of a linear combination of two radial functions at two different energies and one energy derivative (at one of those energies): $\varphi_{lm}^{\mathrm{LO}} = [A_{lm}u_l(r,E_{1,l}) + B_{lm}u_l'(r,E_{1,l}) + C_{lm}u_l(r,E_{2,l})]Y_{lm}(\vec{r})$, where the coefficients A_{lm}, B_{lm}, and C_{lm} are determined by the requirement that $\varphi_{lm}^{\mathrm{LO}}$ should be normalized and has nonzero value and slope at the sphere boundary.
[31] J.P. Perdew, J.A. Chevary, S.H. Vosko, K.A. Jackson, M.R. Pederson, D.J. Singh, and C. Fiolhais, Phys. Rev. B **46**, 6671 (1992).
[32] J.P. Perdew, S. Burke, and M. Ernzerhof, Phys. Rev. Lett. **77**, 3865 (1996).
[33] *Diamagnetic Susceptibility*, Landolt-Börnstein, New Series, Group II, Vol. 16, edited by R. R. Gupta, K.-H. Hellwege, and A. M. Hellwege (Springer-Verlag, Berlin, 1986).
[34] C.E. Moore, *Atomic Energy Levels* (National Bureau of Standards, Washington, DC, 1971).